Impact of sample crushing on porosity characterization of hardened cement pastes by low temperature calorimetry: comparison of powder and cylinder samples

Min Wu[a,*], Katja Fridh[b], Björn Johannesson[c], Mette Geiker[d]

[a]*Department of Civil Engineering, Technical University of Denmark, Building 118, 2800 Lyngby, Denmark*
[b]*Division of Building Materials, Lund University, Lund, Sweden*
[c]*Department of Building Technology, Linnaeus University, Växjö, Sweden*
[d]*Department of Structural Engineering, Norwegian University of Science and Technology, Trondheim, Norway*

Abstract

The impact of sample crushing on the detected porosity of hardened cement pastes by low temperature calorimetry (LTC) was studied using powder and cylinder samples. Two types of cements, CEM I and CEM III, were used to prepare the pastes. A model porous material, MCM-41, was also used in order to investigate some aspects of the measurement and the evaluation approach. The powder and cylinder samples of the cement pastes were compared in terms of the calculated ice content curves, total pore volumes and pore size distribution curves. For the two studied cement pastes, the calculated ice content curves of freezing of the powder sample differed from that of the cylinder samples, especially for the paste CEM III. The results indicate that sample crushing changed the pore connectivity as compared to non-crushed samples. One important difference between the powder sample and the cylinder samples of the paste CEM III was that the determined maximum ice content in the powder sample was much higher than that in the cylinder samples, the relatively difference being about 40-50%. However, this kind of marked difference was not found in the paste CEM I. The observed difference between the calculated pore volume of the powder and the cylinder samples of the paste CEM III is possibly due to some of the "isolated" pores which, presumably, cannot be fully filled with water in the preparation of the cylinder samples. However, sample crushing makes it possible to saturate the pores to a greater

*Corresponding author. The content presented in this article has been included as part of the PhD thesis of the author and archived in the univeristy repository[1]. Current contact address: COWI A/S, Parallelvej 2, 2800 Lyngby, Denmark. Tel: +45 5640 7118.

extent if the crushing contributes to open up the "isolated" pores. Consequently, more pores are detected in the powder samples. The argument that the "isolated" pores have a tendency to be opened up by the crushing process is supported by results using gravimetric measurements and "dynamic (water) vapor sorption" measurements on powder samples.

Keywords: Cement paste, calorimetry, freezing and thawing, pore size distribution, thermoporometry, cryoporometry

1. Introduction

The pore system in a cement based material is very complicated and the pore sizes can range from millimeter scale to nanometric level [2, 3]. The porosity at the nanometric level is of paramount importance in studying properties of cement based materials. It is the main parameter which influences, e.g., the strength, the shrinkage, the transport properties and the durability [4]. Moreover, the properties of the nanometric pores are quite essential in the modeling of some important processes of cement based materials, e.g., moisture transport [5, 6], drying shrinkage [7] and carbonation [8, 9]. Thus, the accuracy of the pore structure characterization of cement based materials is crucial. A number of methods have been used to determine the pore structure of cement based materials, e.g. mercury intrusion porosimetry (MIP) [10, 11], nitrogen adsorption/desorption (NAD) [12], scanning electron microscopy (SEM) [13], water vapor sorption [14], small-angle X-ray scattering [15, 16] and small-angle neutron scattering [17, 18]. Recently, liquid proton Nuclear Magnetic Resonance has been used and interested results have been reported [19, 20].

Low temperature (micro-)calorimetry or LTC, also known as thermoporometry and sometimes referred to as thermoporosimetry or cryoporometry [21], is one of the used methods to investigate the porosity of materials, especially pores at the meso-level, i.e., pores with widths between 2 and 50 nm, according to the IUPAC definition [22, 23]. LTC has been used extensively to study the porosity of cement based materials, e.g., in [21, 24–26]. Compared with the traditional methods developed for porosity characterization, e.g., mercury intrusion porosimetry (MIP), nitrogen adsorption/desorption (NAD) and scanning electron microscopy (SEM), a major advantage of using LTC on cement based materials is that the measurements can be conducted on virgin samples without any drying treatment [21, 26–28], as the drying treatment in many cases results in an alteration of the pore structure of cement based materials [29, 30].

As for most of the techniques, LTC is an indirect method for porosity determination. The analysis of the measured data is not straightforward and special care should be taken in the data analysis. In LTC studies, e.g., using water as the probe liquid, the instrument records the heat flow during the freezing and melting process. Based

on the measured heat flow, the ice content in a sample at different temperatures can be calculated. To calculate the ice content, the baseline must be determined carefully and appropriate values of the heat of fusion of the water/ice confined in small pores at different temperatures must be specified. The impact of the two factors, i.e., the baseline determination and the values of the heat of fusion of confined water/ice, on the calculated ice content has been presented in an earlier study [31]. To calculate the pore size distribution, the relation between the pore size and the depressed freezing/melting point must be known. Under certain basic assumptions, thermodynamic considerations demonstrate that there is a unique equation between the phase transition temperature of the water/ice confined in pores and the curvature of its solid-liquid interface [32, 33]. The quantitative relation of the freezing/melting point and the pore size can be principally determined by adopting appropriate values for the thermodynamic parameters of the confined water/ice. However, there is no generally consensus on which values should be used for the thermodynamic parameters of water confined in pores, especially at low temperatures, e.g., the surface tension, the heat of fusion and the heat capacity of water and ice [22, 33, 34]. This makes the quantitative determination of the relation between the freezing/melting point and the pore size difficult. Additionally, it should be mentioned that the samples to be tested in LTC studies need to be fully saturated by the probe liquid. If the samples are not fully saturated, the total pore volume will be underestimated since the LTC method can only detect the pores filled with the probe liquid. Moreover, the relation between the depressed freezing/melting temperature and the pore size in this context is normally derived based on the prerequisite that the pores under study are fully saturated. It has been shown that the needed thermodynamic relations to be used for fully saturated pores are different from that for non-fully saturated pores [35]. The needed thermodynamic relations for a non-fully saturated pore system are very complicated, and therefore difficult to determine quantitatively, if it is still possible at all. The impact of using the thermodynamic relations as derived based on fully saturation for non-fully saturated system on the determined pore size distribution is discussed in [35].

Due to the constraints as discussed above, it should be mentioned that similar to many other indirect methods, LTC is a semi-empirical method for pore structure characterization. This is considered especially true when working with materials like hardened cement pastes, where the pore structures are very complicated as discussed above. To our knowledge, perhaps at this moment there is no method, which can determine the "real" or "true" pore structure of materials with complicate pore systems at nanometric level. Most of the indirect methods, if not all of them, are no more than semi-quantitative.

In LTC studies, the freezing of pore water is normally assumed to be a process initiated by heterogeneous nucleation and then followed by progressive penetration [36, 37].

That is, the freezing process after the heterogeneous nucleation, i.e., the ice penetration process, is controlled by the pore entry or neck sizes; while the melting process is controlled by the pore interior sizes [26, 38]. For this reason, the freezing process indicates the pore connectivity and the melting process reflects the pore interior size distribution. It is noted that in some LTC studies on cement based materials, the sample size is either relatively small (with the mass on the order of tens of milligrams), e.g., see [39], or relatively big (with the mass on the order of several grams), e.g, see [21], depending on the instrument adopted. For LTC measurements on samples with relatively small size, crushing and sometimes even grinding is needed in sample preparation. The procedure of sample crushing and/or grinding is also needed in sorption studies using a "Dynamic water vapor sorption (DVS)" instrument due to small sample holder. In sorption studies, it is normally pre-assumed that the crushing and/or grinding of the cement paste samples do not change the pore structure at the nanometric level, e.g., see [14, 40]. However, it should be mentioned that there are NMR cryoporometry studies, e.g., see [41, 42], which compares the measurements on the same material but in different forms, i.e., big integral and crushed samples. The results show that the pore connectivity is changed by the sample crushing even though the pore interior size distribution remains about the same. The impact of sample crushing, i.e., using different size of samples, in LTC studies on the determined porosity of hardened cement pastes is, however, not fully clear and needs to be further examined.

This work aims to clarify the possible impact of sample crushing on the pore structures of hardened cement pastes characterized by LTC. Hardened cement paste samples prepared from two types of cements are included. For each hardened cement paste, two types of samples, i.e., in the form of powders and cylinders, are used. One mono-sized model material MCM-41 is also included in this study. MCM-41 is a silica based material and the pore structure is in the form of hexagonal arrays of uniform tubular channels of controlled width, which has been widely used as a model material in the context of porosity characterization [43–46].The purposes of including the model material MCM-41 are two folds: firstly, it is to validate the stability of the instrument; secondly, it is to validate the applicability of the LTC in the context of porosity determination (By comparing the analyzed results from our experiments with that provided by supplier, the aim is to validate the LTC method, including the data evaluation method adopted in the study, is applicable). By doing this, it is expected that the possible effects due to the instrument and data evaluation method, which may lead to differences in the obtained results, can be excluded. In this way, the difference noted between powders and cylinders of studied hardened cement pastes can be attributed to the sample crushing. The impact of sample crushing on the detected porosity of the studied hardened cement pastes is demonstrated and some possible explanations are proposed for the observed differences.

2. Experimental

2.1. Materials preparation

2.1.1. Model material MCM-41

The MCM-41 used in this study is in the powder form and is produced by Tianjin Chemist Scientific Ltd. The nominal pore diameter and the total pore volume reported by the producer are 3.0 nm and $\geq$ 0.70 ml/g, respectively.

In order to handle powders more easily in the instrument during calorimetric measurements (Section 2.2), a cylindrical plastic vial was used as a sample holder the powder sample. The size of the plastic vials ($\sim \phi 14 \times 48$ mm) was chosen to fit the measuring chamber of the calorimeter. The MCM-41 powders were placed into the plastic vials up to about half the volume (the dry weight was about 0.2 g) and then covered with distilled water. In order to saturate the samples, the plastic vials containing powders covered with distilled water were placed under a reduced pressure ($\sim$ 40 mbar) for about 3 hours. After that, the apparent excess bulk water on top of the powders was removed and the samples were stored in closed containers for two to three weeks before calorimetric measurements.

2.1.2. Cement pastes

Two types of cements, i.e., CEM I 32.5 R and CEM III/B 42.5 N, were used to prepare paste samples in this study. Refer to AppendixA for the properties and the chemical composition of the cements . The water-to-cement ratio of the prepared paste samples was 0.4. A paddle mixer was used to mix the fresh pastes. After mixing, the fresh pastes were cast into cylindrical plastic vials followed by proper compaction. The dimension of the plastic vials is about $\phi 15 \times 50$ mm. The hardened cement pastes were demoulded after one day of sealed curing at room temperature (about 20 °C). Following the demoulding, the paste samples were placed into slightly bigger plastic flasks ($\sim \phi 25 \times 60$ mm) filled with saturated limewater for curing at room temperature. As the pore solution of hardened cement pastes contains many ionic species [47], using pure water for curing may lead to leaching of ions from hydration products as reported in, e.g., [48]. It is a recommended practice to cure cement based materials with saturated limewater, e.g. see [49].

The cylinder samples of the hardened cement pastes were used to obtain powder samples. The cylinders were firstly vacuum saturated with saturated limewater and then the crushing and grinding of the samples were conducted in a carbon dioxide free chamber. Cement based materials exposed to air will carbonate, which will lead to the change of the microstructure [50]. Therefore, carbon dioxide free chamber was used to avoid carbonation. After that, the ground paste powders (passed through 315 μm sieve) were placed into the plastic vials up to about half the volume and then covered with saturated limewater. This procedure was also conducted in the carbon dioxide

free chamber. Following that, the plastic vials containing cement paste powders were placed under reduced pressure for saturation purpose (as did for the MCM-41 powders in Section 2.1.1). After the saturation, the apparent excess bulk water on top of the powders was removed and the samples were stored in closed containers for two to three weeks before calorimetric measurements (after calorimetric measurements, the dry weight of cement paste powders and the total water content in each plastic vial were determined as about 1:1).

For cylinder samples of the cement pastes, they were vacuum saturated and then the apparent bulk water on the surface of cylinders was wiped off before calorimetric measurements.

When calorimetric measurements were performed, the total curing time of the cylinder and powder samples of the studied cement pastes were about 1 year and 1.5 years, respectively.

By using two types of cements, part of the effect due to cement types on the porosity determination by LTC is expected to be observed. The hardened cement pastes are designated as CEM I and CEM III in the following discussion.

2.2. Calorimetric measurements

A Calvet-type scanning calorimeter (SETARAM) was used in this investigation. The calorimeter was calibrated and operated to work between about 20 °C down to about -130 °C. The cooling and heating rate were set to be 0.1 °C per minute. A freezing and melting cycle consists the temperature scanning starting from about 20 °C and going down to about -80 °C and then back to about 20 °C again. The cooling and heating rates were adopted based on suggestions given in [51, 52], where both stability of the measured results and efficiency of the measurements were considered. The rates are in the same order as recommended by, e.g., [24], for the same type of instrument.

In the measurements of the powder samples, a plastic vial same as the sample holder but empty was placed in the reference chamber of the calorimeter. The purpose was to counteract the effects due to some uncertainties that the plastic vial may experience during freezing and melting measurements. In the measurements of the cylinder cement paste samples, a totally dry paste sample (oven drying at about 105 °C until constant weight) of the same dimension as the testing specimen was used as a reference sample in the LTC instrument. One purpose of using the reference sample is to reduce the possible uncertainties of the solid paste during the freezing and melting measurements. More discussions about the influence and the benefits of using such a reference sample in calorimetric measurements can be found in [31, 52].

Due to the energetic barrier to nucleation, bulk water can be cooled down below 0 °C without freezing, i.e., the supercooling behavior [34]. Because of the supercooling, it

is then not possible to derive any pore entry information from the freezing curves during the temperature range between 0 °C and the point when the supercooling terminates (the initial nucleation starts). In order to suppress the supercooling of water during freezing and to derive more information from the freezing process in LTC studies, two cycles of freezing and melting measurements have been suggested, e.g, see [23, 26, 53]. Following the same concept, a trial run of a two cycles of freezing and melting using the employed instrument was conducted. However, the results showed that in this study, no more useful information can be obtained compared with the case of using one freezing and melting cycle, refer to AppendixB for more explanation and details. Therefore, only one freezing and melting cycle was used for all the measurements.

The mass of the tested vacuum saturated samples before and after calorimetric measurements were determined. The relative difference of the mass is less than about 0.15%. That is, there is almost no water loss during the calorimetric measurements. After calorimetric measurements, the tested samples were oven-dried at about 105 °C until constant weight to obtain the dry weights. The total water content of each sample was obtained by the mass difference between the dry state and the state before the calorimetric measurement.

For the model material MCM-41, calorimetric measurements were performed on two samples of the same kind. By doing this, the stability of the instrument was expected to be validated (assuming the MCM-41 powders are homogenous as they were collected from a rather big batch). For the cylinder samples of each cement paste, three different samples were measured with the purpose to check the homogeneity of the prepared cylinder samples. The powder samples of each investigated cement paste were collected from two cylinders and the homogeneity was not further checked. That is, only one calorimetric measurement was conducted on the powder samples of each studied cement paste.

Additionally, using vacuum saturated samples, the total porosity of the cylinder samples of the two studied cement pastes were also determined through gravimetric measurements by recording the mass of the samples both in air and submerged in water.

3. Results and discussion

3.1. Ice content

The ice content calculation based on the measured data of heat flow is central for pore volume and pore size distribution determination in LTC studies. Special care should be taken in determining the baseline of heat flow and choosing the appropriate values for the thermodynamic parameters of water/ice confined in pores, i.e., surface tension, heat capacity and heat of fusion. A summary of the calculation methods/procedures is presented in AppendixC. Detailed discussions in this context and

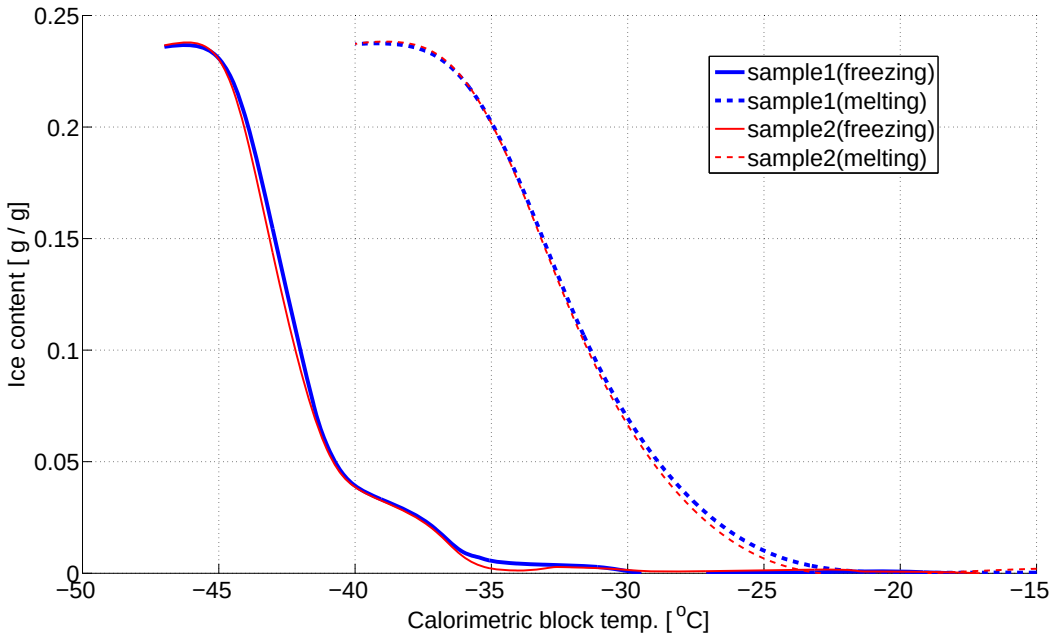

Figure 1: Calculated ice content curves of the two measured samples of the model material MCM-41 (with excess bulk ice subtracted). The ice content is expressed as gram per gram of dry material.

the methods for ice content calculation can be found in [31]. The "C-baseline" method together with the values chosen for the relevant parameters as discussed in [31], which has been demonstrated suitable to calculate the ice content, is used in this study.

3.1.1. Model material MCM-41

The calculated ice content curves of the two measured samples of the model material MCM-41 are shown in Figure 1. It can be found that the difference between the ice content curves (both freezing and melting) of the two samples is small. That is, the stability of the instrument is concluded to be satisfactory.

3.1.2. Cement pastes

For the cement pastes CEM I and CEM III, the calculated ice content curves for the measured three cylinder samples and one powder sample of each paste are presented in Figure 2 and Figure 3, respectively. It should be mentioned that the presented ice content does not include the "bulk" ice, which is determined by calculating the ice content corresponding to the peak above 0 °C from the heat flow curve of melting. For the cylinder samples, the "bulk" ice is mainly the ice in big pores (with small temperature depression, e.g., air voids) since saturated surface dry samples were used; while for the powder samples, the "bulk" ice should contain both the ice in big pores

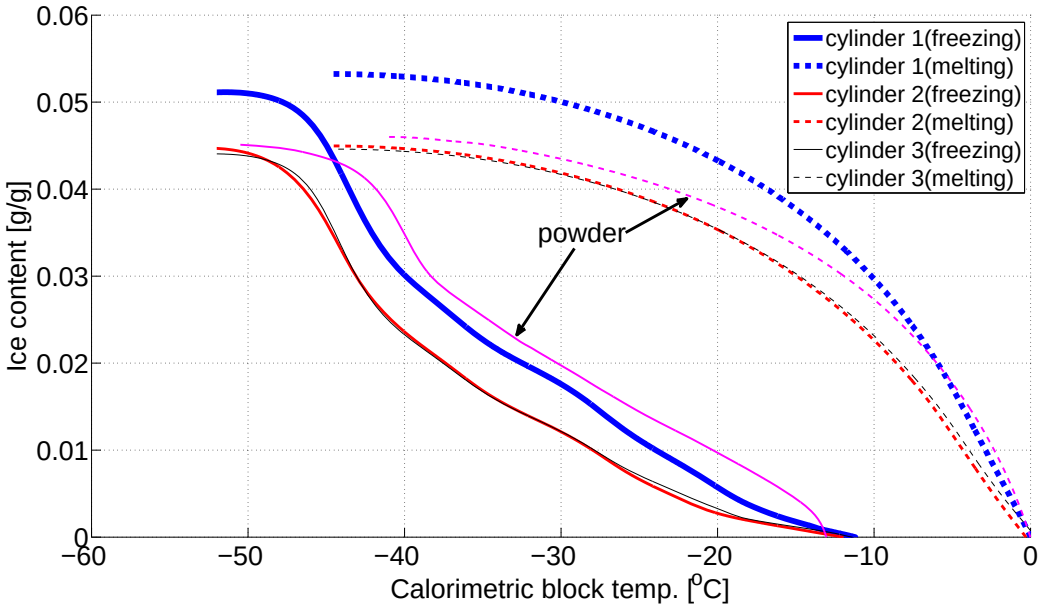

Figure 2: Calculated ice content curves of cylinder and powder samples of the cement paste CEM I (with "bulk" ice subtracted). The content of "bulk" ice in each sample is determined by calculating the ice content corresponding to the peak above 0 °C from the heat flow curve of melting. The ice content is expressed as gram per gram of dry material.

and the excess bulk water since there is still a portion of excess water in the powder samples as determined.

As can be found from Figure 2, for the paste CEM I, the calculated ice content curves of two of the measured three cylinder samples (cylinder 2 and cylinder 3) are quite comparable; while the ice content curves of one sample (cylinder 1) differ from that of the other two to a certain extent. Since the instrument is rather stable (according to the measurements on the MCM-41, see Figure 1), the difference between the ice content curves as determined for the cylinder samples is attributed to the inhomogeneity of the prepared samples. For the powder sample of the paste CEM I, the ice content curve during melting is higher than that of cylinder 2 and cylinder 3 at a same temperature while it is generally lower compared with that of the cylinder 1 (except during the temperature range between -7 °C and about 0 °C). There are two main differences between the ice content curves of freezing of the powder sample and the cylinder samples. Firstly, the ice content curve of freezing of the powder sample starts at a somewhat lower temperature than that of the cylinders. That is because the starting point of the ice content curve of freezing reflects the heterogeneous nucleation temperature (of supercooled water) and it generally decreases as the sample size decreases [54]. Secondly, the ice content curve of freezing of the powder sample

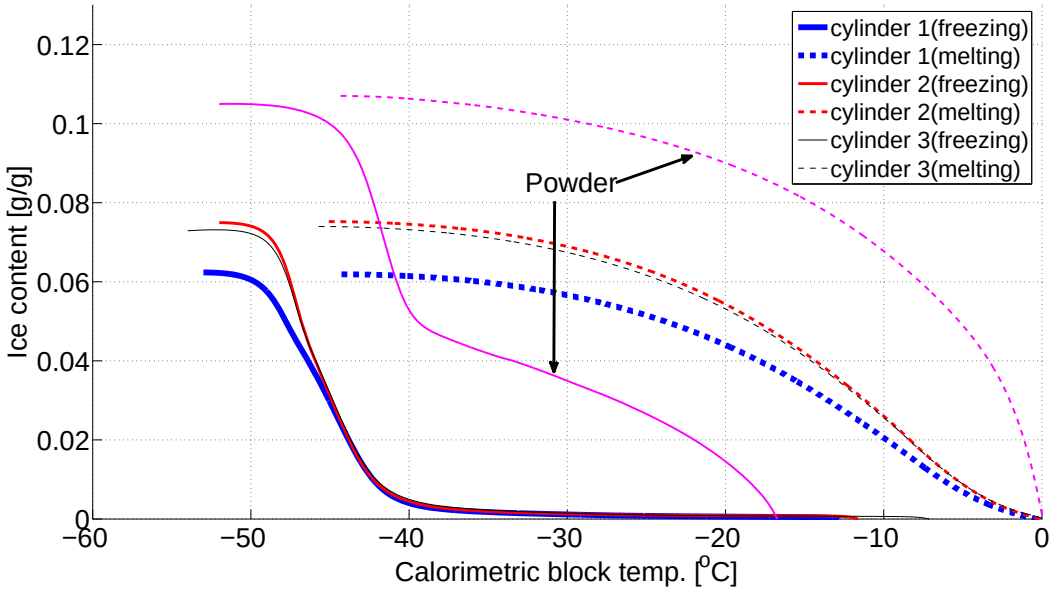

Figure 3: Calculated ice content curves of cylinder and powder samples of the cement paste CEM III (with "bulk" ice subtracted). The content of "bulk" ice in each sample is determined by calculating the ice content corresponding to the peak above 0 °C from the heat flow curve of melting. The ice content is expressed as gram per gram of dry material.

is higher than that of all the three cylinders at a same temperature. The more ice content detected at a same temperature during freezing indicates that the connectivity of the pores in the powder sample is increased compared with that of the cylinders, i.e., more pores are penetrable by ice at a same temperature. The increased connectivity of the powder sample is more obvious by comparing the ice content curve of freezing of the powder sample with that of cylinder 1. Even though cylinder 1 has a higher pore volume than the powder sample (i.e., reflected by a higher maximum ice content), the ice content curve of freezing of the powder sample is still higher than that of the cylinder sample at a same temperature. The results may indicate that the crushing of cylinder samples into powders increases the pore connectivity.

Some differences as found between the powder sample and the cylinder samples for the paste CEM I are also found for the paste CEM III (Figure 3), e.g., the inhomogeneity of the prepared cylinder samples and the increased pore connectivity in the powder sample than that in the cylinder samples. There are also some new features. The difference between the ice content curve of freezing of the powder sample and that of the cylinder samples for the paste CEM III is more significant compared with that of the paste CEM I. From the ice content curves of freezing of the paste CEM III (Figure 3), it should be mentioned that the freezing behavior of the water in cylinder samples

is quite different from that in the powder sample. When the temperature goes down to about -40 °C, very limited amount of ice is formed in the cylinder samples while about half of the total ice is formed in the powder sample. As we know, the freezing process is an ice penetration process (after the initial heterogeneous nucleation) controlled by pore entry sizes. That is, the pore entry sizes in cylinder samples of the paste CEM III can be very small and ice cannot penetrate through the small pore entries. Only when the temperature goes down to a very low point when homogenous nucleation becomes significant (e.g., about -40 °C) , will the pore water then freeze irrespective of pore sizes. While for the powder sample, ice has already penetrated into the sample and occupied about half of the total pore volume when the temperature goes down to about -40 °C. The comparison of the ice content curves of freezing between the powder sample and cylinder samples of the paste CEM III indicates that the crushing of cylinder samples into powders may significantly change the pore connectivity.

Another important difference between the powder sample and the cylinder samples of the paste CEM III is that the determined maximum ice content in the powder sample is much higher compared with that in the cylinder samples. The relatively difference is up to about 40-50%. However, the marked difference is not found from the comparison of the paste CEM I (Figure 2).

The marked difference of the determined maximum ice content between the cylinder and powder samples of the paste CEM III (indicating more pores detected in the powder sample) may be related to the "isolated" pores. It should be mentioned that in LTC studies on cement based materials, there is normally a peak starting at around -40 °C (and it is extended to lower temperatures) on the measured freezing heat flow curves and this peak is often associated with the so-called "isolated" pores, e.g., see [21, 38, 55]. Then two types of "isolated" pores can be envisaged: (1) totally isolated pores (which may form due to, e.g., self-desiccation during the hydration); (2) pores connected to very small pore entries in which water does not freeze above about -40 °C, i.e., pores "isolated" by small pore entries. It could be that some of the "isolated" pores in the cylinder samples cannot be fully saturated with water during vacuum saturation due to a very complicated pore structure, e.g., of which pores are less connected and the whole pore system is quite tortuous; while in the powder sample, due to the increased pore connectivity as a result of the sample crushing, some of the initially "isolated" pores can be opened and then they are able to be filled with water during vacuum saturation. Consequently, the overall saturation degree of the "isolated" pores in the powder sample after vacuum saturation could be much higher compared with that in the cylinder samples. Since LTC detects only the water filled pores, it is not surprising that more pores are detected in the powder sample, as observed in Figure 3. The impact of sample crushing on the "isolated" pores is schematically illustrated in Figure 4 (the small amount of water in the "isolated" pores, i.e., pore A and pore B in Figure

4a and pore C in Figure 4b, is schematic, which may come from, e.g., diffusion and/or unreacted mixing water)[1].

The much more marked difference of the ice content between the powder and cylinder samples as found in the paste CEM III (Figure 3) compared with that in the paste CEM I (Figure 2) may indicate that there are probably more "isolated" pores in the paste CEM III than that in the paste CEM I. Combined with the calculated total pore volume, more discussions about the impact of the sample crushing on the detected porosity will be conducted in Section 3.2.

From the comparison of the ice content curves for the powder and cylinder samples of the studied cement pastes, it can be concluded that the crushing of a sample into powders increases the pore connectivity. Another important consequence of sample crushing is that it could possibly result into more pores detected by LTC in the crushed powders than that in a big sample, with one possible reason being that the saturation degree of the "isolated" pores in a big sample can be greatly increased after the crushing during saturation.

3.2. Total pore volume

The total content of pore water (more accurately, it is ice and the unfreezable water in pores) in each LTC studied sample is calculated by subtracting the content of "bulk" ice (as explained in Section 3.1) from the determined total water content. Further assuming the density of pore ice/water as 1.0 g/ml, the total pore volume of each LTC studied sample is estimated[2]. For the materials measured more than once in this study, the total pore volume is obtained by averaging that of the several measurements. The total pore volume of the LTC studied samples are listed in Table 1. The porosity of the model material MCM-41 and the pastes CEM I and CEM III were also studied by the Dynamic (water) Vapor Sorption (DVS) measurement [58]. The DVS results, together with that of the gravimetric measurements, are also listed in Table 1.

[1] In Figure 4, the "isolated" pores are inside of a rather big hardened cement paste (e.g., a cylinder sample). During vacuum saturation, water may have no access to the totally isolated pores, e.g., in (a) and probably small pore entries may block or prevent water from penetrating into the "isolated" pores, e.g., in (b). However, if the sample is crushed along any line between pore A and pore B, e.g., the line *d*, then all the "isolated" pores are more easily to be filled with water during saturation (corresponding to powder samples).

[2] The density of ice is temperature dependent [56], see Eq.C.1. As the density difference in the concerned temperature range (0 °C to about -40 °C) is less than 1.0%, the temperature dependence is not considered in the estimation for the sake of simplicity. As the density of ice is less than 1.0 g/ml [56] and maybe for unfreezable pore water as well [57], this assumption probably results into underestimation of the pore volume, with the error being not greater than about 8.0% of the estimated value .

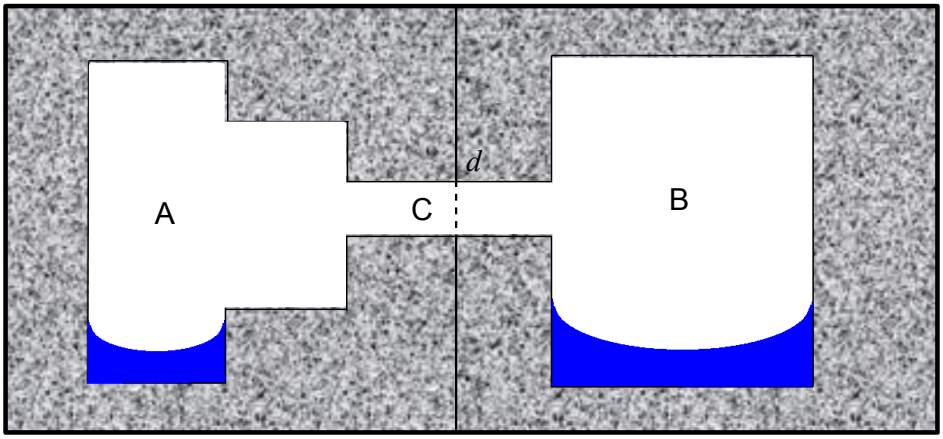

(a)

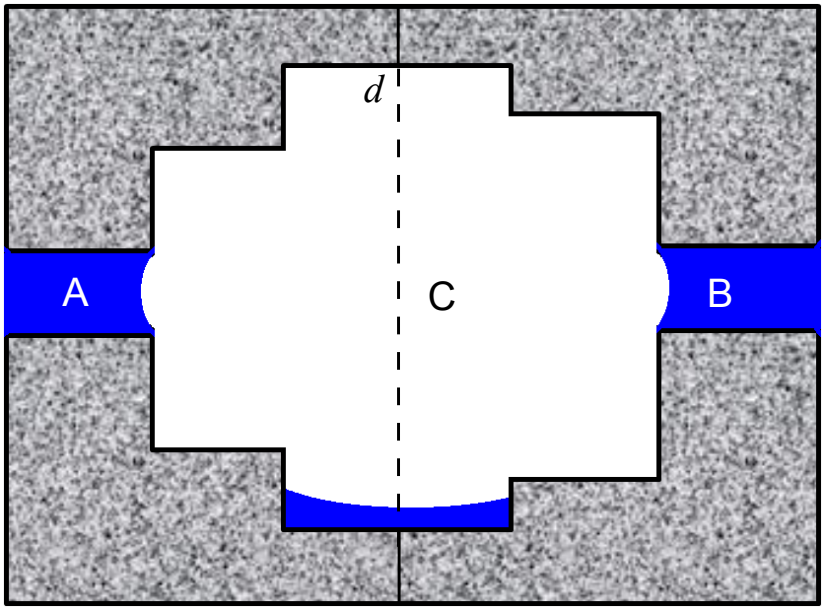

(b)

Figure 4: A schematic illustration of "isolated" pores. (a) pore A, pore B and pore C are three connected but totally isolated pores; (b) pore C is connected to but kind of "isolated" by pore A and pore B with very small sizes.

Table 1: Total pore volume of the MCM-41 and the pastes CEM I and CEM III obtained from different methods. The values are expressed in the unit of milliliter per gram dry material (ml/g).

		LTC[a]	Gravimetric measurement[b]	DVS[b,c,d]
MCM-41		0.72	-	0.77
CEM I	cylinder	0.20	0.21	-
	powder	0.21	-	0.20
CEM III	cylinder	0.23	0.23	-
	powder	0.29	-	0.35

Note: (a). the volume of the big pores (e.g., air voids, as explained in Section 3.1) in the cement pastes is not included. From the calculation on the cylinder samples, the volume of the the big pores in pastes CEM I and CEM III is about 0.007 and 0.003 ml/g, respectively; (b). density of pore water is assumed to be 1.0 g/ml; (c). moisture content determined during desorption at the RH of 0.95 which is almost the upper limit that the instrument can work with; d). the age of the cement pastes is about 6-8 months when measured.

As can be seen from the results presented in Table 1, the total pore volume of the paste CEM I obtained from different methods are comparable. For the paste CEM III, the total pore volume determined from the gravimetric measurements is comparable to that of the cylinder samples by LTC; while the total pore volume determined from DVS, which is much higher than that of the cylinder samples by LTC, is more comparable to that of the powder sample by LTC. The comparison between the results obtained from the gravimetric and the DVS measurement for the cement paste CEM III is in agreement with that of the results obtained from LTC studies on the powder and cylinder samples, i.e., the sample crushing is concluded to have an impact on the detectable pore volume. However, by noting that the differences between the results found for the paste CEM III using different samples are not observed on the paste CEM I, it should be mentioned that the effect of the sample crushing is probably dependent on the (porosity) properties of the studied material.

3.3. Pore size distribution

With the obtained ice content curves of the freezing and the melting process as presented in Section 3.1, it is possible to calculate both the pore entry size and the pore interior size distribution of the studied material. Refer to AppendixC for explanation of the calculation procedures.

For the measured samples in this study, it should be mentioned that the meaningful temperature range of the freezing curves that can be used to calculate the pore entry sizes is only from around -10 °C to about -40 °C. The pores with entry sizes bigger

than that corresponding to a temperature depression of about -10 °C are not detected because of supercooling. That is, no ice has been formed before reaching about -10°C and hence no calculation can be made. When the temperature goes down to about -40 °C, the homogenous nucleation becomes significant [36, 37, 59] and all the freezable pore water would freeze independent of the pore (entry) sizes. That is, the ice formed around the homogenous nucleation temperature does not indicate any pore size information. For the MCM-41, the pore (entry) size is too small to be obtained from the freezing curve as the main ice content is formed below about -40 °C. For the studied cement pastes, the pore entry radii that can be obtained are between about 2.4 nm to about 5-6 nm (using Eq.C.1). As the obtained pore (entry) size range is quite limited from the ice content curves of freezing of the cement pastes, the results are not presented. In the following, only the ice content curves of melting are used to calculate the pore interior size distribution.

3.3.1. Model material MCM-41

For the model material MCM-41, the mean ice content of the two measured samples (melting curves) as presented in Figure 1 is used for the calculation of the pore size distribution. The thermal lag between the calorimetric block and a tested sample is assumed to be negligible. The calculated pore size distribution (PSD) curves of the MCM-41 are presented in Figure 5. The pore radius corresponding to the peak in the calculated PSD curves, sometimes referred to as the most frequent pore radius R_{max} [60], is about 1.7 nm and 2.7 nm assuming cylindrical and spherical pores, respectively. It should be mentioned that the pores of MCM-41 products are often assumed to be very close to cylindrical shape [43, 44, 46, 61]. Including the spherical shape assumption in the calculation is for comparison purpose only. The R_{max} of 1.7 nm based on the cylindrical pore assumption is close to the value provided by the producer, i.e., the diameter of 3.0 nm.

3.3.2. Cement pastes

For the cylinder samples of each cement paste, the representative ice content is calculated by averaging the results of the three cylinder samples (melting curves) of each paste (Figure 2 and Figure 3). One may argue that the thermal lag for the cylinder samples might be different from that for the powder sample. If the thermal lag is different, it should be more obvious at very low temperatures. For all the measured cement paste samples, there is a characteristic peak corresponding to homogenous nucleation, which starts around -40 °C and is extended to several degrees lower, on the heat flow curves of freezing [55, 62]. By comparing the starting temperature of the characteristic peak due to homogenous nucleation on the heating flow curves of freezing, it is concluded that the thermal lag for the cylinder samples and the powder sample are close, if there is any. One may also argue that the ionic concentration in

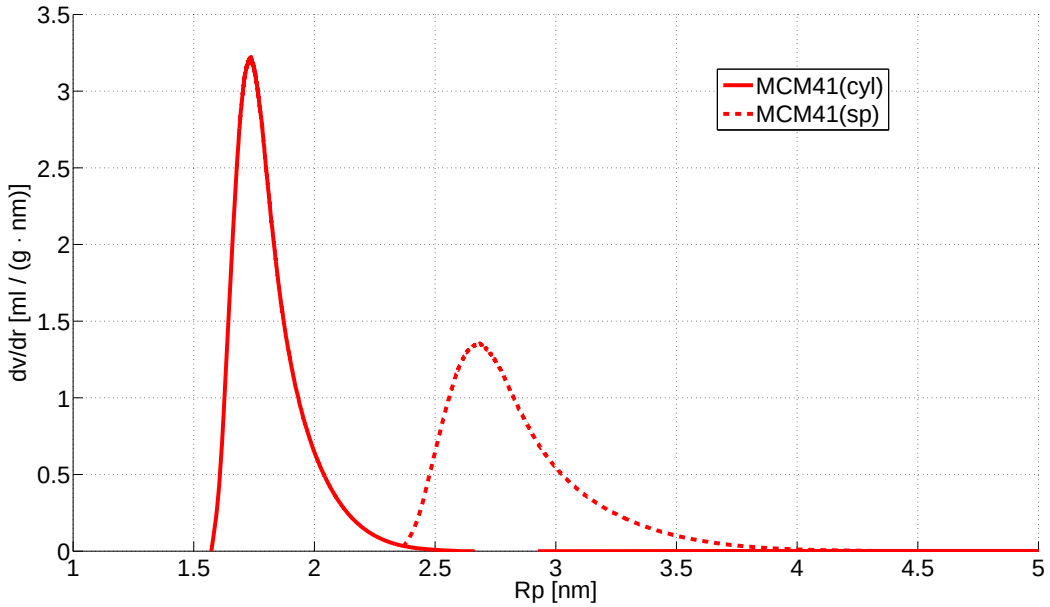

Figure 5: Calculated differential pore size distribution of the model material MCM-41 based on the cylindrical (cyl) and the spherical (sp) pore assumption.

the pore solution might be different, since the water content in the powder sample is higher than that in the cylinder samples. A study [62] indicates that the amount of curing water has very limited effect in changing the freezing and melting behaviors of the cement pore solution. In this study, it is therefore assumed that the impact of the ions on the freezing and melting point depression for the cylinder samples and the powder sample are more or less the same. In this investigation, both the thermal lag and the effect due to ions are not considered.

The calculated accumulated and differential PSD curves for the pastes CEM I and CEM III are shown in Figure 6 and Figure 7, respectively. It can be found that the calculated accumulated PSD curves of the powder sample are generally higher than that of the cylinder sample, especially for the paste CEM III (Figure 7a), indicating that the volume of the relatively big pores is higher in the powder sample. However, from the calculated differential PSD curves, it is found that the portion of small pores, i.e., with the radii between about 2 to 10 nm for the paste CEM I and the radii between about 2 to 5-6 nm (depending on the pore shape assumption) for the paste CEM III, is relatively higher in the cylinder sample.

More big pores found in the powder sample compared to the cylindrical ones may attribute to that the sample crushing opens some "isolated" pores which may be not fully filled with water before crushing but can be fully saturated after crushing (Section 3.1). Thus, more pores are detected using the powder sample. For the more small

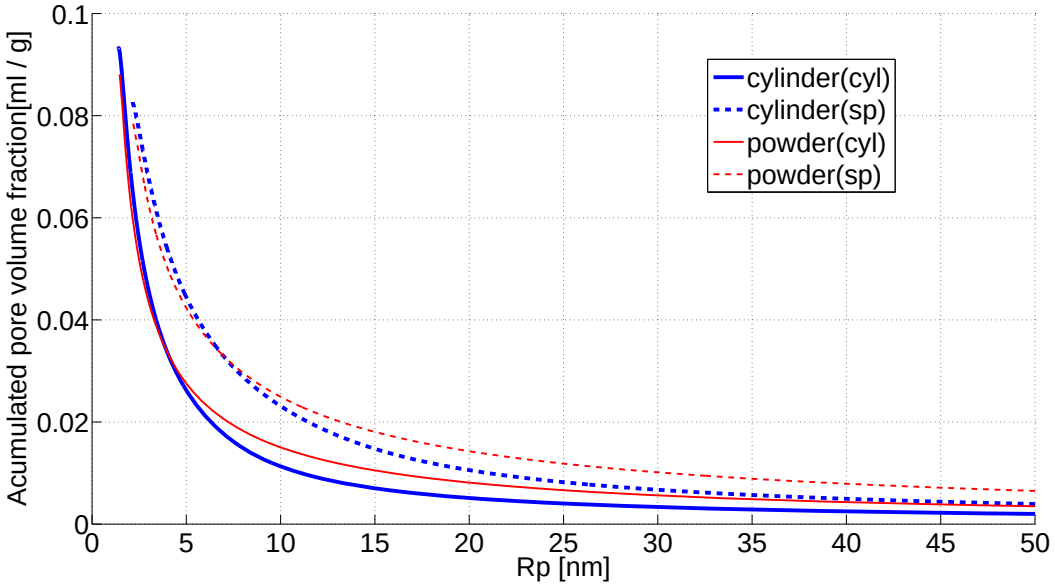

(a) Accumulated pore size distribution

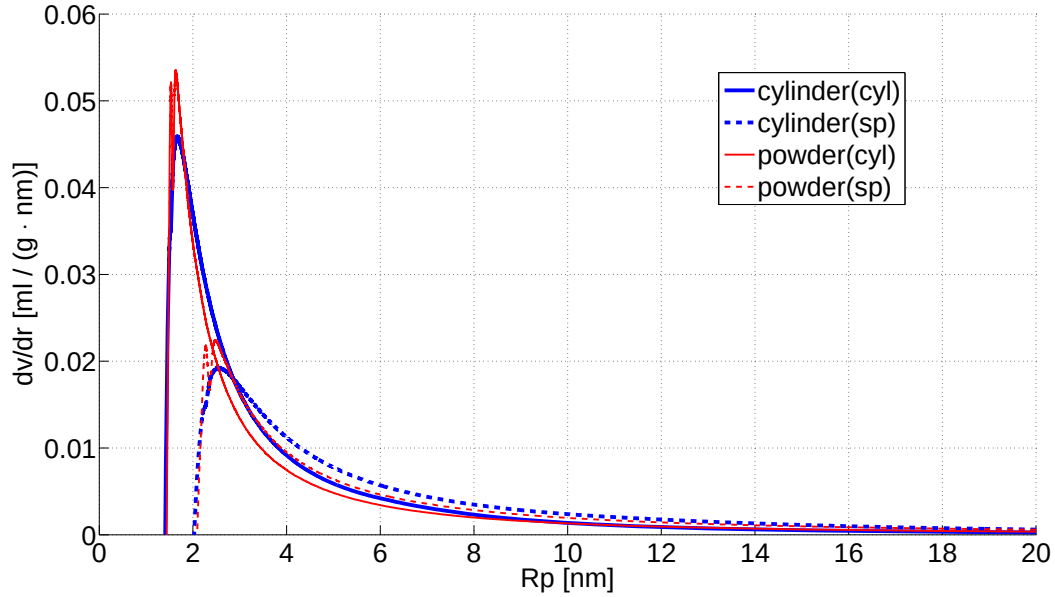

(b) Differential pore size distribution

Figure 6: Calculated accumulated and differential pore size distribution curves of cylinder and powder samples of the cement paste CEM I. The pore shape is assumed to be cylindrical (cyl) or spherical (sp).

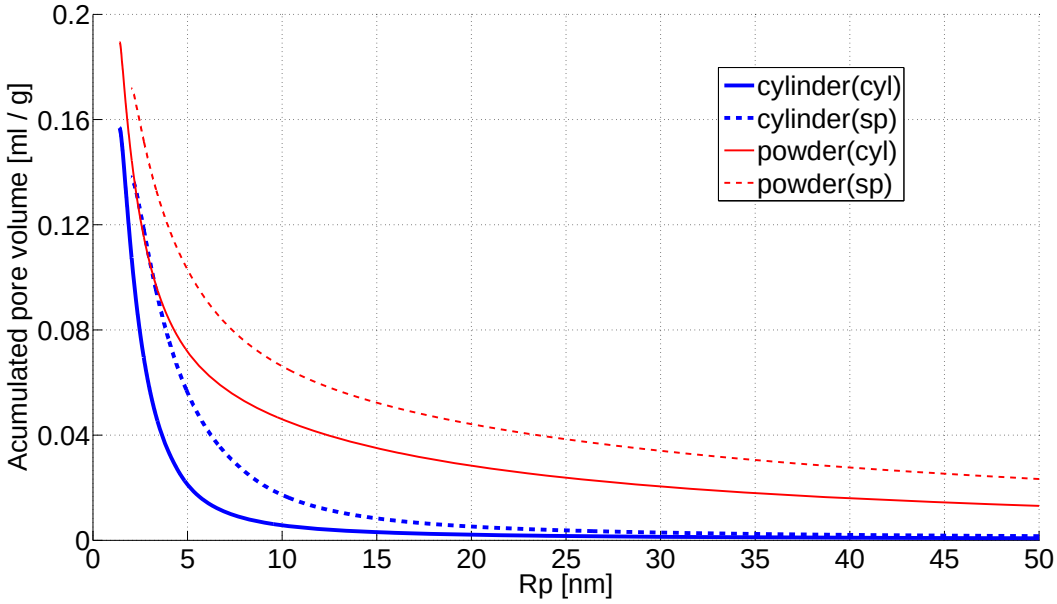

(a) Accumulated pore size distribution

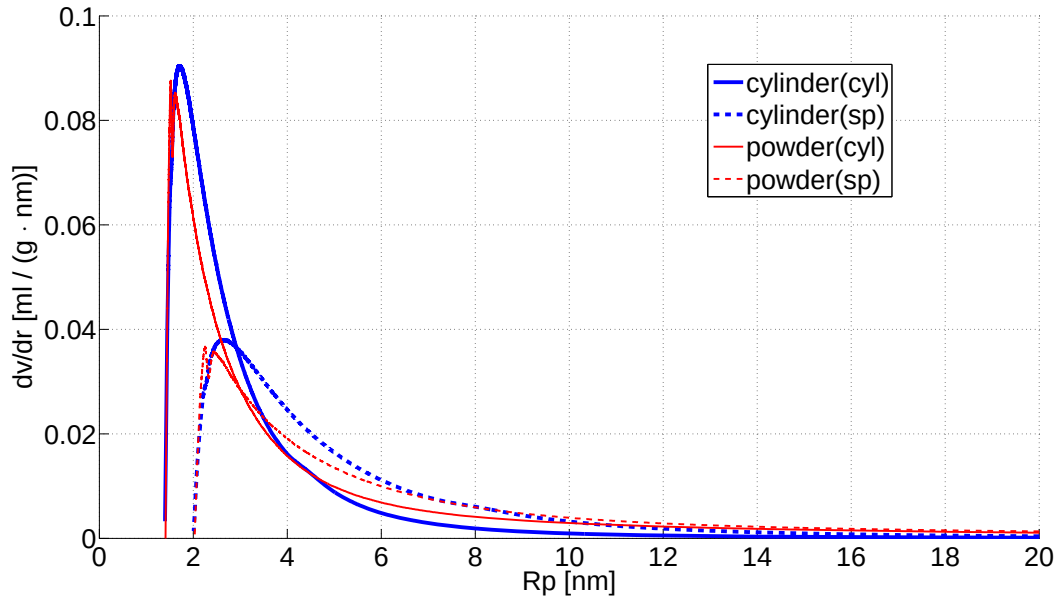

(b) Differential pore size distribution

Figure 7: Calculated accumulated and differential pore size distribution curves of cylinder and powder samples of the cement paste CEM III. The pore shape is assumed to be cylindrical (cyl) or spherical (sp).

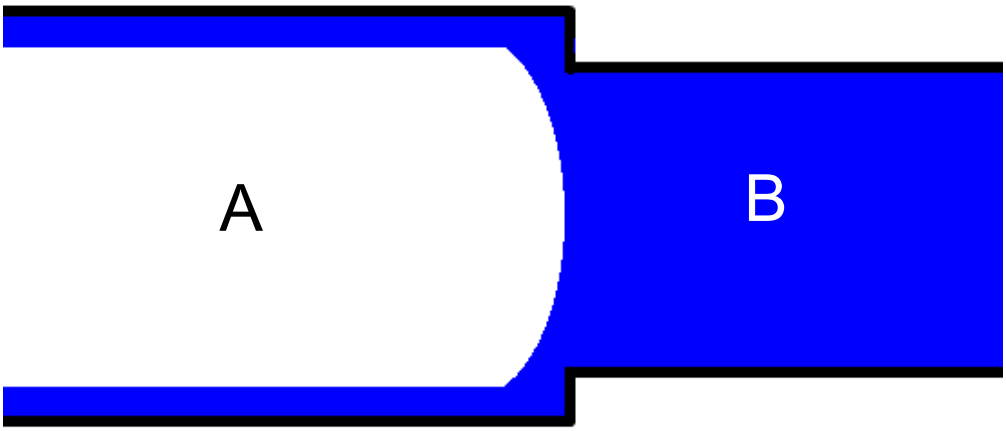

Figure 8: A schematic illustration of the concept of advanced melting, based on the description from [26, 42], refer to Footnote 3 for explanation.

pores in the cylinder samples observed from the calculated differential PSD curves, it is possibly related to the so-called advanced melting phenomenon [42, 63]. It is normally assumed that for cylindrical pores, the melting would take place in a radical direction [42], or melting from the side (the direction perpendicular to the diameter) [26]. However, melting could also take place from the end (the direction parallel to the diameter), depending on the pore size and connectivity [26, 42]. If melting initiates from the end, it is the so-called advanced melting. The concept of advanced melting is schematically shown in Figure 8[3]. Since the sample crushing changes the connectivity

[3] In Figure 8, pore A and B are two cylindrical pores and connected co-axially, with radii $R_A > R_B$. If the melting initiates from the side (the direction from left to right in the drawing), the ice in pore B will melt at a temperature corresponding to $1/(R_B - \delta)$ and then in pore A at a temperature corresponding to $1/(R_A - \delta)$, where δ is the thickness of the unfreezable layer close to the pore wall. That is, the ice in pore A will melt at a higher temperature compared with the ice in pore B (the smaller the curvature, the higher the melting point). But as pore A and B are connected, the melting point of the ice in pore A also depends on the size relation of the two pores. Considering the case when the ice in pore B melts, the water in pore B is in equilibrium with a ice/water interface having a curvature infinitesimally smaller than $1/(R_B - \delta)$. The ice in pore A terminates in a hemispherical cap with a curvature of $2/(R_A - \delta)$. If $2/(R_A - \delta) \geq 1/(\mathrm{R}_B - \delta) = 2/[2(R_B - \delta)]$, i.e., approximately $R_A < 2R_B$ (assuming δ is smaller than R_A and R_B), then the ice hemispherical cap is not thermodynamically stable in pore A and the ice in pore A will melt from the end (the direction from top to bottom in the drawing). That is, due to the connectivity of the two pores and if $R_B < R_A < 2R_B$, the ice in pore A could melt from the end rather than from the side. This is the so-called advanced melting phenomenon. In such a case, the melting point of the ice in pore A from the end (corresponding to the curvature of pore B melting, $1/(R_B - \delta)$) is lower than that from the side (corresponding to the curvature of pore A melting, $1/(R_A - \delta)$). Using the same calculation (Eq.C.3, which assumes melting from the side), some big pores may be wrongly calculated as small pores due to the advanced melting.

of the pores, the impact of advanced melting on the powder and the cylinder samples may be different. One consequence of the advanced melting on the pore size distribution determination is that big pores may be wrongly calculated as small pores [42], which can somewhat explain the difference between the calculated volume of small pores in the powder and the cylinder samples. Additionally, some of the "isolated" pores in cylinder samples may be not fully saturated as mentioned earlier (Section 3.1). It has been demonstrated in [35] that the freezing/melting point of the water/ice confined in the non-fully saturated pores will be further depressed compared with the condition that the pores are fully saturated. The effect is that the calculated sizes of the pores under non-fully saturation are underestimated. Thus, it could also explain that there are more (calculated or apparent) small pores in the powder sample than what found in the cylinder sample as observed for the studied pastes.

4. Conclusions

Two types of samples, i.e., in the form of powder and cylinder, were used to study the impact of sample crushing on the detected porosity of hardened cement pastes by low temperature calorimetry (LTC). The studied cement pastes were prepared by two types of cements. The difference between the powder and cylinder samples was compared in terms of the calculated ice content curves, total pore volumes and pore size distribution curves.

For the studied cement pastes, the calculated ice content curves of freezing of the powder sample differed from that of the cylinder samples, especially for the paste CEM III. It indicated that sample crushing changed the pore connectivity. Another important difference between the powder sample and the cylinder samples of the paste CEM III was that the determined maximum ice content in the powder sample was much higher compared with that in the cylinder samples, the relatively difference being about 40-50%. However, this kind of marked difference was not found from the comparison of the powder and cylinder samples of the paste CEM I. That is, sample crushing could possibly result into more pores detected by LTC depending on the (porosity) characteristic properties of the studied paste.

About the marked difference between the calculated pore volume of the powder and the cylinder samples of the paste CEM III, one possible reason could be that some of the "isolated" pores which, presumably, cannot be fully filled with water in the preparation of the cylinder samples. However, sample crushing makes it possible to saturate the pores to a greater extent if the crushing contributes to open up the "isolated" pores. Consequently, more pores can be detected in the powder samples. The argument about the "isolated" pores is supported by the results of gravimetric measurements on cylinder samples and the DVS measurements on powder samples.

Acknowledgments

The research leading to these results has received funding from the European Union Seventh Framework Programme (FP7/2007-2013) under grant agreement 264448. A part of this research was funded by the Lizzy, Alfred and Valdemar Taumose's Foundation. The authors would like to thank Stefan Backe from the Division of Building Materials of Lund University for performing some of the tests.

AppendixA. Properties and the chemical composition of cements

The properties and the chemical composition of the cements used in this study are shown in Table A.1.

Table A.1: Properties and the chemical composition of the two cements used in this study.

		CEM I (CEM I 32.5 R)	CEM III (CEM III/B 42.5 N)
Density	(g/cm^3)	3.06	2.90
Fineness	(cm^2/g)	2905	4635
Water demand	(%)	26.2	32.3
Initial setting time	(min)	185	270
Loss on ignition	(%)	2.1	1.4
SiO_2	(%)	20.6	29.2
Al_2O_3	(%)	5.6	8.9
Fe_2O_3	(%)	2.4	1.2
CaO	(%)	63.4	48.0
MgO	(%)	1.6	4.8
SO_3	(%)	2.9	2.6
K_2O	(%)	0.7	0.6
Na_2O	(%)	0.2	0.2
Cl	(%)	<0.1	<0.1

AppendixB. Trial run of two cycles of freezing and melting processes

As mention in Section 2.2, two cycles of freezing and melting measurements have been suggested in the context of LTC studies, e.g, see [23, 26, 53]. The first freezing process is to create some ice crystals and the first melting process is run up to just below the melting point of macroscopic ice (i.e., the ice in big air voids or on the external surfaces of the testing sample), e.g., that the samples were heated to -0.05 °C in [26] and about -0.5 °C in [53]. The macroscopic ice formed in the first freezing process,

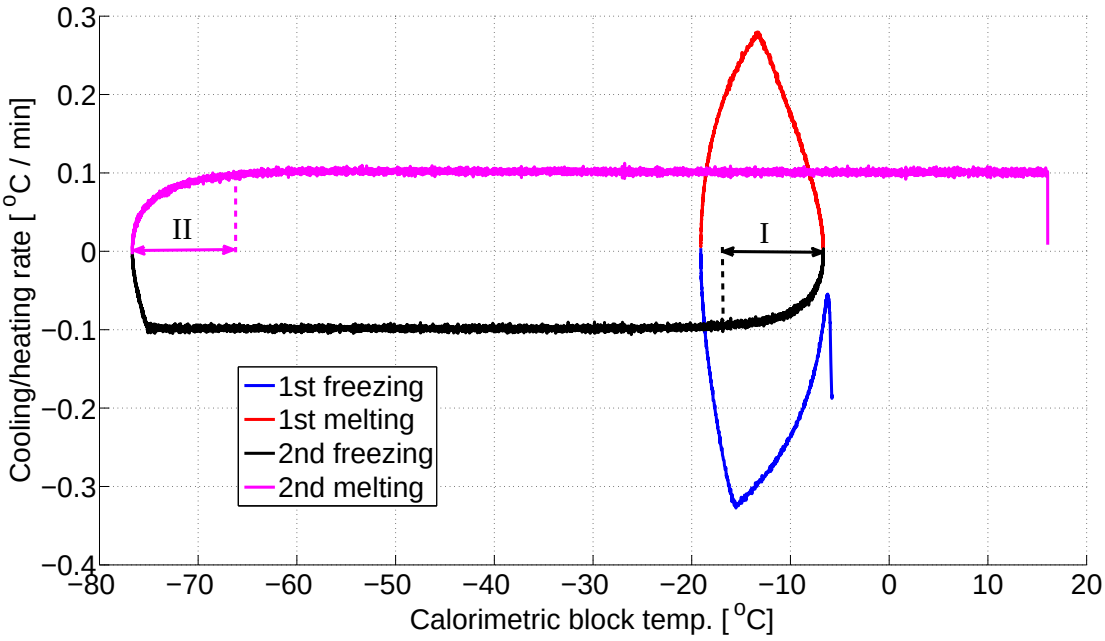

Figure B.1: The cooling/heating rates during a trial run of two cycles of freezing and melting using the employed instrument.

which serves as the ice front, then penetrates through the pore network of the sample during the second freezing process. By adopting the two cycles procedure, the pore entry and interior sizes can be obtained from the second freezing and melting process, respectively.

A trial run of a two cycles of freezing and melting using the employed instrument was conducted. The first cycle was run on a relatively high cooling/heating rate, as suggested in [23, 26, 53], since the main purpose is just to create some macroscopic ice to be used in the second cycle. The second cycle was run on the set cooling/heating rate for measurements, i.e., 0.1 °C per minute. The cooling/heating rates during the trial run are calculated and shown in Figure B.1. It is found that it would take about 10 °C for the cooling/heating rate to be stabilized when the process is changed from cooling to heating and *vice versa* (as indicated by notation I and II in Figure B.1). The importance of the stability of the cooling/heating rate during measurements in the ice content determination has been discussed in [31]. That is, the ice content during the temperatures with unstable cooling/heating rate may not be calculated properly. Assuming the testing samples are successfully heated up to just slightly lower than 0 °C in the first melting process and then the samples are cooled down immediately, the ice content of the second freezing during the temperature from about 0 °C to about -10 °C may not be obtained properly, due to the unstable cooling rate during the temperature

range. As will be shown later, measurements on the cylinder samples of cement pastes using one freezing and melting cycle show that the supercooling also terminates at around -10 °C (see Figure 2 and Figure 3). Similar to the two cycles of measurement, the ice content of the freezing process during the temperature from about 0 °C to about -10 °C also cannot be obtained. That is, using two cycles cannot provide more pore entry information (derived from the ice content curve of the freezing process) compared with that using one cycle. Thus, only one freezing and melting cycle was used for all the measurements.

In summary, the benefit of using a two cycles of freezing and melting in the context of LTC studies can only be guaranteed if the cooling/heating rate of the instrument, when changing the process from cooling to heating, and *vice versa,* can be stabilized rather quickly, i.e., notation I and II as indicated in Figure B.1 covering a short temperature range. In this study, limited added value can be obtained by using the two cycles since it will take about 10 °C for the cooling/heating rate to be stabilized when changing the process. Consequently, only one freezing and melting cycle was adopted to improve the efficiency of measurements.

AppendixC. LTC data interpretation procedures

The typical output measured by LTC experiments is the relation between heat flow and the temperature, e.g., see Figure C.1. To derive pore size information, several steps would be needed. The essential parts of the data interpretation procedures including necessary assumptions have been explained in a detailed manner in previous studies [31, 35]. The main steps, together with important assumptions, are listed below. Interested readers are advised to find more details in [31, 35].

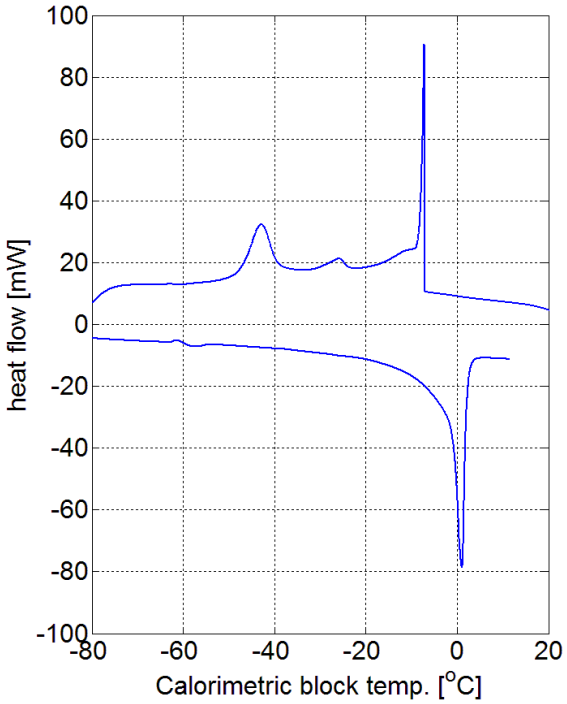

Figure C.1: Typical output from LTC measurements, i.e., the relation between heat flow and the temperature.

1. Calculate ice content from the heat flow curve
   (a) Baseline calculation

   The heat flow measured by a LTC instrument consists of two parts: (1) the contribution from the heat capacity of the system (including water and ice in the concrete sample, and also the concrete skeleton matrix), which is referred to as the "heat flow baseline" or simply "baseline" in this discussion; and (2) the contribution due to the phase transition. Hence, in order to calculate the ice content, one needs to know how much energy goes to form or melt ice at each temperature level, which basically is obtained by subtracting the baseline from the measured total heat flow. The determination of the baseline is complicated by the facts that the heat flow is continuously changing due to the change in the proportion of ice and liquid water confined in the pores and the temperature dependent heat capacities of water, ice and the solid matrix.

   We propose two different methods, i.e., the "J-baseline" method and the "C-baseline" method. The "J-baseline" method is a recently proposed method based on extrapolation by using the accumulated heat curves measured in the freezing and the melting process. The "C-baseline" method considers

the heat capacity of both water and ice and the phase changing behavior under the different testing temperatures. Refer to [31] for the advantages and constraints of each method.

(b) Ice content calculation

With the obtained baseline, we know how much heat is related to phase change of the water/ice. By dividing the heat related to phase change by the heat of fusion of water, the ice content can be calculated.

It should be noted that the water/ice under study in this case is the water/ice confined in small pores. Although bulk water/ice is relatively well studied, there is no general agreement on how to obtain the important temperature dependence of the heat of fusion of water/ice confined in small pores. In this study, the values of the heat of fusion of water as proposed in, e.g., Ishikiriyama et al. [22, 53, 57, 64], are used. Refer to [31] for reasons and discussion.

2. Derive pore size information from the calculated ice content

(a) Pore volume calculation

From Step 1, we know the ice content corresponding to each temperature level. Dividing the calculated ice contents (in mass) by the ice density, we get the ice volume. The density of ice adopted in the pore size distribution calculation is a temperature dependent function, which is [56]

$$\rho_{ice} \approx 0.9167 - 2.053 \cdot 10^{-4}\theta - 1.357 \cdot 10^{-6}\theta^2 \qquad \text{g/ml} \qquad \text{(C.1)}$$

where θ is the temperature in Celsius degree.

(b) It should be noted that it is normally assumed that there is a portion of water which is very close to the pore walls and it will not undergo phase transition even if the temperature is very low. This unfreezable layer, referred to as $\delta-$layer, is normally treated as consisting of 2-3 layers of water molecules, which corresponds to about 0.8 nm in thickness, e.g., in [33, 53, 65]. The calculated ice volume plus the volume of this unfreezable layer of water is the pore volume.

(c) Pore size calculation

To calculate the pore sizes, thermodynamic relation between the depressed freezing point of water confined in a pore and the pore size should be used, e.g., see [23, 32, 33, 36].. In addition, assumptions have to be made with respect to pore shape. In this study, the classical assumptions of cylindrical pores and spherical pores are followed. It is well acknowledged that the real pore size/shape of cement paste materials is rather complicated and the actual pore shape may deviate significantly from the ideal pore shape

assumed. However, with no better generally accepted model, the cylindrical and spherical pore shape assumptions are used.

Based on different pore shape assumption and the process (either freezing or melting), Brun et al. [33] proposed two equations accounting for the relation between the pore size and the freezing/melting depression. The two equations are used in this study, i.e.,

$$R_p = -\frac{64.67}{T - T_0} + 0.57 \tag{C.2}$$

$$R_p = -\frac{32.33}{T - T_0} + 0.68 \tag{C.3}$$

where R_p (nm) is the pore size; T and T_0 is the freezing/melting point of pore water/ice and bulk water/ice, respectively. For the cylindrical pore assumption, Eq.C.2 is used for the freezing process and Eq.C.3 is used for the melting process; while for spherical pore assumption, Eq.C.2 is used for both the freezing and the melting process.

(d) With the obtained pore volume and pore size at each corresponding temperature level, the pore size distributions (e.g., differential and accumulated) can be calculated.

Reference

[1] M. Wu. *Using low temperature calorimetry and moisture fixation method to study the pore structure of cement based materials*. PhD thesis, Technical University of Denmark, Department of Civil Engineering, 2014. URL http://orbit.dtu.dk/files/103261580/Min_Wu_Thesis.pdf.

[2] S.H. Kosmatka and W.C. Panarese. *Design and control of concrete mixtures*. Portland Cement Association, 2002.

[3] H.M. Jennings. Refinements to colloid model of C–S–H in cement: CM–II. *Cement and Concrete Research*, 38(3):275–289, 2008.

[4] H.F.W. Taylor. *Cement chemistry*. Thomas Telford, London, 2nd edition, 1997.

[5] V. Baroghel-Bouny. Water vapour sorption experiments on hardened cementitious materials. Part II: Essential tool for assessment of transport properties and for durability prediction. *Cement and Concrete Research*, 37(3):438–454, 2007.

[6] V. Baroghel-Bouny, M. Mainguy, and O. Coussy. Isothermal drying process in weakly permeable cementitious materials- assessment of water permeability. In *International Conference on Ion and Mass Transport in Cement-Based Materials*, pages 59–80, 1999.

[7] V. Baroghel-Bouny, M. Mainguy, T. Lassabatere, and O. Coussy. Characterization and identification of equilibrium and transfer moisture properties for ordinary and high-performance cementitious materials. *Cement and Concrete Research*, 29(8): 1225–1238, 1999.

[8] M. Thiery, V. Baroghel-Bouny, G. Villain, and P. Dangla. Numerical modeling of concrete carbonation based on durability indicators. In V.M. Malhotra, editor, *Proceedings of the 7th CANMET/ACI International Conference on Durability of Concrete*, pages 765–780, 2006.

[9] B. Bary and A. Sellier. Coupled moisture–carbon dioxide–calcium transfer model for carbonation of concrete. *Cement and Concrete Research*, 34(10):1859–1872, 2004.

[10] S. Diamond. Mercury porosimetry: an inappropriate method for the measurement of pore size distributions in cement-based materials. *Cement and Concrete Research*, 30(10):1517–1525, 2000.

[11] C Gallé. Effect of drying on cement-based materials pore structure as identified by mercury intrusion porosimetry: a comparative study between oven-, vacuum-, and freeze-drying. *Cement and Concrete Research*, 31(10):1467–1477, 2001.

[12] M. Juenger and H. Jennings. The use of nitrogen adsorption to assess the microstructure of cement paste. *Cement and Concrete Research*, 31(6):883–892, 2001.

[13] P. Stutzman. Scanning electron microscopy imaging of hydraulic cement microstructure. *Cement and Concrete Composites*, 26(8):957–966, 2004.

[14] V. Baroghel-Bouny. Water vapour sorption experiments on hardened cementitious materials: Part I: Essential tool for analysis of hygral behaviour and its relation to pore structure. *Cement and Concrete Research*, 37(3):414–437, 2007.

[15] D.N. Winslow and S. Diamond. Specific surface of hardened portland cement paste as determined by small-angle X-ray scattering. *Journal of the American Ceramic Society*, 57(5):193–197, 1974.

[16] M. Kriechbaum, G. Degovics, J. Tritthart, and P. Laggner. Fractal structure of portland cement paste during age hardening analyzed by small-angle x-ray scattering. In *Trends in Colloid and Interface Science III*, pages 101–105. Springer, 1989.

[17] A. Allen and J. Thomas. Analysis of c–s–h gel and cement paste by small-angle neutron scattering. *Cement and Concrete Research*, 37(3):319–324, 2007.

[18] D. Pearson and A.J. Allen. A study of ultrafine porosity in hydrated cements using small angle neutron scattering. *Journal of Materials Science*, 20(1):303–315, 1985.

[19] P.J. McDonald, V. Rodin, and A. Valori. Characterisation of intra-and inter-C–S–H gel pore water in white cement based on an analysis of NMR signal amplitudes as a function of water content. *Cement and Concrete Research*, 40(12):1656–1663, 2010.

[20] A.C.A. Muller, K.L. Scrivener, A.M. Gajewicz, and P.J. McDonald. Densification of C-S-H measured by ^{1}H NMR relaxometry. *The Journal of Physical Chemistry C*, 117(1):403–412, 2012.

[21] A.M. Kjeldsen and M.R. Geiker. On the interpretation of low temperature calorimetry data. *Materials and Structures*, 41(1):213–224, 2008.

[22] K. Ishikiriyama and M. Todoki. Pore size distribution measurements of silica gels by means of differential scanning calorimetry II. thermoporosimetry. *Journal of Colloid and Interface Science*, 171(1):103–111, 1995.

[23] M.R. Landry. Thermoporometry by differential scanning calorimetry: experimental considerations and applications. *Thermochimica Acta*, 433(1-2):27–50, 2005.

[24] D.H. Bager. *Ice Formation in Hardened Cement Paste*. PhD thesis, Building Materials Laboratory, Technical University of Denmark, 1984.

[25] D.H. Bager and E.J. Sellevold. Ice formation in hardened cement paste, Part III-slow resaturation of room temperature cured pastes. *Cement and Concrete Research*, 17(1):1–11, 1987.

[26] Z. Sun and G.W. Scherer. Pore size and shape in mortar by thermoporometry. *Cement and Concrete Research*, 40(5):740–751, 2010.

[27] D.H. Bager and E.J. Sellevold. Ice formation in hardened cement paste, Part I–room temperature cured pastes with variable moisture contents. *Cement and Concrete Research*, 16(5):709–720, 1986.

[28] E. Sellevold and D. Bager. Some implications of calorimetric ice formation results for frost reistance testing of concrete. *in Beton og Frost, Dansk Beton Forening*, 22:47–74, 1985.

[29] J. Villadsen. Pore structure in cement based materials. Technical Report 277, Building Materials Laboratory, Technical University, Denmark, 1992.

[30] R. Espinosa and L. Franke. Influence of the age and drying process on pore structure and sorption isotherms of hardened cement paste. *Cement and Concrete Research*, 36(10):1969–1984, 2006.

[31] M. Wu, B. Johannesson, and M. Geiker. Determination of ice content in hardened concrete by low temperature calorimetry: influence of baseline calculation and heat of fusion of confined water. *Journal of Thermal Analysis and Calorimetry*, 115(2): 1335–1351, 2014.

[32] R. Defay, I. Prigogine, A. Bellemans, and D.H Everett. *Surface tension and adsorption*. Longmans London, 1966.

[33] M. Brun, A. Lallemand, J.F. Quinson, and C. Eyraud. A new method for the simultaneous determination of the size and shape of pores: the thermoporometry. *Thermochimica Acta*, 21(1):59–88, 1977.

[34] D.M. Murphy and T. Koop. Review of the vapour pressures of ice and supercooled water for atmospheric applications. *Quarterly Journal of the Royal Meteorological Society*, 131(608):1539–1565, 2005.

[35] M. Wu and B. Johannesson. Impact of sample saturation on the detected porosity of hardened concrete using low temperature calorimetry. *Thermochimica Acta*, 580: 66–78, 2014.

[36] G.W. Scherer. Freezing gels. *Journal of non-crystalline solids*, 155(1):1–25, 1993.

[37] D.H. Rasmussen and A.P. MacKenzie. Clustering in supercooled water. *The Journal of Chemical Physics*, 59:5003, 1973.

[38] G. Fagerlund. Determination of pore-size distribution from freezing-point depression. *Materials and Structures*, 6(3):215–225, 1973.

[39] D. Bentz and P. Stutzman. Curing, hydration, and microstructure of cement paste. *ACI Materials Journal*, 103(5):348–356, 2006.

[40] M. Åhs. *Redistribution of moisture and ions in cement based materials*. PhD thesis, Division of Building Materials, Lund University, 2011.

[41] E.L. Perkins, J.P. Lowe, K.J. Edler, N. Tanko, and S.P. Rigby. Determination of the percolation properties and pore connectivity for mesoporous solids using NMR cryodiffusometry. *Chemical Engineering Science*, 63(7):1929–1940, 2008.

[42] E. Shiko, K.J. Edler, J.P. Lowe, and S.P. Rigby. Probing the impact of advanced melting and advanced adsorption phenomena on the accuracy of pore size distributions from cryoporometry and adsorption using NMR relaxometry and diffusometry. *Journal of Colloid and Interface Science*, 385(1):183–192, 2012.

[43] P.J. Branton, P.G. Hall, K.S.W. Sing, H. Reichert, F. Schüth, and K.K. Unger. Physisorption of argon, nitrogen and oxygen by MCM-41, a model mesoporous adsorbent. *J. Chem. Soc., Faraday Trans.*, 90(19):2965–2967, 1994.

[44] P.J. Branton, P.G. Hall, and K.S.W. Sing. Physisorption of alcohols and water vapour by MCM-41, a model mesoporous adsorbent. *Adsorption*, 1(1):77–82, 1995.

[45] P.I. Ravikovitch, S.C.Ó. Domhnaill, A.V. Neimark, F. Schüth, and K.K. Unger. Capillary hysteresis in nanopores: theoretical and experimental studies of nitrogen adsorption on MCM-41. *Langmuir*, 11(12):4765–4772, 1995.

[46] J. Banys, M. Kinka, J. Macutkevic, G. Völkel, W. Böhlmann, V. Umamaheswari, M. Hartmann, and A. Pöppl. Broadband dielectric spectroscopy of water confined in MCM–41 molecular sieve materials–low-temperature freezing phenomena. *Journal of Physics: Condensed Matter*, 17:2843, 2005.

[47] M. Wu, B. Johannesson, and M. Geiker. A preliminary study of the influence of ions in the pore solution of hardened cement pastes on the porosity determination by low temperature calorimetry. *Thermochimica Acta*, 589:215–225, 2014.

[48] K. Haga, S. Sutou, M. Hironaga, S. Tanaka, and S. Nagasaki. Effects of porosity on leaching of Ca from hardened ordinary portland cement paste. *Cement and Concrete Research*, 35(9):1764–1775, 2005. doi: http://dx.doi.org/10.1016/j.cemconres.2004.06.034.

[49] ASTM C192: Standard Practice for Making and Curing Concrete Test Specimens in the Laboratory. ASTM International, West Conshohocken, 2014.

[50] B. Johannesson and P. Utgenannt. Microstructural changes caused by carbonation of cement mortar. *Cement and Concrete Research*, 31(6):925–931, 2001.

[51] K. Fridh. *Internal frost damage in concrete–experimental studies of destruction mechanisms*. PhD thesis, Division of Building Materials, Lund Institute of Technology, 2005.

[52] B. Johannesson. Dimensional and ice content changes of hardened concrete at different freezing and thawing temperatures. *Cement and Concrete Composites*, 32(1):73–83, 2010.

[53] K. Ishikiriyama, M. Todoki, and K. Motomura. Pore size distribution (PSD) measurements of silica gels by means of differential scanning calorimetry I. optimization for determination of PSD. *Journal of Colloid and Interface Science*, 171 (1):92–102, 1995.

[54] Z. Sun and G.W. Scherer. Effect of air voids on salt scaling and internal freezing. *Cement and Concrete Research*, 40(2):260–270, 2010.

[55] J.P. Kaufmann. Experimental identification of ice formation in small concrete pores. *Cement and Concrete Research*, 34(8):1421–1427, 2004.

[56] R. L. David, editor. *CRC Handbook of Chemistry and Physics*. CRC Press, 83rd edition, 2002.

[57] K. Ishikiriyama and M. Todoki. Evaluation of water in silica pores using differential scanning calorimetry. *Thermochimica Acta*, 256(2):213–226, 1995.

[58] M. Wu, B. Johannesson, and M. Geiker. Application of water vapor sorption measurements for porosity characterization of hardened cement pastes. *Construction and Building Materials*, 66:621–633, 2014.

[59] H.H.G. Jellinek, editor. *Water Structure at the Water-Polymer Interface*. Plenum, New York, 1972.

[60] O. Šolcová, L. Matějová, and P. Schneider. Pore-size distributions from nitrogen adsorption revisited: Models comparison with controlled-pore glasses. *Applied Catalysis A: General*, 313(2):167–176, 2006.

[61] P.J. Branton, K.S.W. Sing, and J.W. White. Adsorption of carbon tetrachloride and nitrogen by 3.4 nm pore diameter siliceous MCM-41. *J. Chem. Soc., Faraday Trans.*, 93(13):2337–2340, 1997.

[62] M. Wu, K. Fridh, B. Johannesson, and M. Geiker. Influence of frost damage and sample preconditioning on the porosity characterization of cement based materials using low temperature calorimetry. *Thermochimica Acta*, 607:30–38, 2015.

[63] I. Hitchcock, E.M. Holt, J.P. Lowe, and S.P. Rigby. Studies of freezing–melting hysteresis in cryoporometry scanning loop experiments using NMR diffusometry and relaxometry. *Chemical Engineering Science*, 66(4):582–592, 2011.

[64] K. Ishikiriyama, M. Todoki, K.H. Min, S. Yonemori, and M. Noshiro. Pore size distribution measurements for microporous glass using differential scanning calorimetry. *Journal of Thermal Analysis and Calorimetry*, 46(3-4):1177–1189, 1996.

[65] T. Yamamoto, A. Endo, Y. Inagi, T. Ohmori, and M. Nakaiwa. Evaluation of thermoporometry for characterization of mesoporous materials. *Journal of Colloid and Interface Science*, 284(2):614–620, 2005.